JOURNAL OF GEOPHYSICAL RESEARCH, VOL. 115, D12111, doi:10.1029/2009JD012674, 2010



# Interannual variability of surface water extent at the global scale, 1993–2004

F. Papa,[1] C. Prigent,[2] F. Aires,[3] C. Jimenez,[2] W. B. Rossow,[1] and E. Matthews[4]

Received 18 June 2009; revised 19 October 2009; accepted 26 January 2010; published 19 June 2010.

[1] Land surface waters play a primary role in the global water cycle and climate. As a consequence, there is a widespread demand for accurate and long-term quantitative observations of their distribution over the whole globe. This study presents the first global data set that quantifies the monthly distribution of surface water extent at ~25 km sampling intervals over 12 years (1993–2004). These estimates, generated from complementary multiple-satellite observations, including passive (Special Sensor Microwave Imager) and active (ERS scatterometer) microwaves along with visible and near-infrared imagery (advanced very high-resolution radiometer; AVHRR), were first developed over 1993–2000. The ERS encountered technical problems in 2001 and the processing scheme had to be adapted to extend the time series. Here we investigate and discuss the adjustments of the methodology, compare the various options, and show that the data set can be extended with good confidence beyond 2000, using ERS and AVHRR mean monthly climatologies. In addition to a large seasonal and interannual variability, the new results show a slight overall decrease in global inundated area between 1993 and 2004, representing an ~5.7% reduction of the mean annual maximum in 12 years. The decrease is mainly observed in the tropics during the 1990s. Over inland water bodies and large river basins, we assess the variability of the surface water extent against related variables such as in situ river discharges, altimeter-derived and in situ river/floodplain water level heights, and precipitation estimates. This new 12 year data set of global surface water extent represents an unprecedented source of information for future hydrological or methane modeling.

**Citation:** Papa, F., C. Prigent, F. Aires, C. Jimenez, W. B. Rossow, and E. Matthews (2010), Interannual variability of surface water extent at the global scale, 1993–2004, *J. Geophys. Res.*, *115*, D12111, doi:10.1029/2009JD012674.

## 1. Introduction and Background

[2] Terrestrial waters on Earth's ice-free land represent less than 1% of the total amount of water on Earth. However, they have a strong impact on life and the human environment. Among the various reservoirs in which fresh water is stored on land (e.g., ice caps, glaciers, snow pack, soil moisture, groundwater), surface waters, comprising rivers, lakes, reservoirs, wetlands, and episodically inundated areas, play a crucial role in the global biochemical and hydrological cycles [*Alsdorf et al.*, 2007a], with a significant influence on the climate variability.

[3] From a biogeochemical point of view, wetlands and inundation events have a major impact on methane production, carbon storage and release, denitrification, and sulfur cycles. They are the world's dominant natural source of methane ($CH_4$) and the only one dominated by climate variations. Approximately 20%–40% of the world's total annual methane emission to the atmosphere comes from natural wetlands and irrigated (seasonally flooded) rice fields [*Houweling et al.*, 1999; *Matthews*, 2000; *Gedney et al.*, 2004], hence the fluctuations in wetlands and inundation extents are key contributors to the interannual variability in methane surface emissions [*Bousquet et al.*, 2006; *Ringeval et al.*, 2010]. Natural wetlands are also an important source and sink of $CO_2$, with still ambiguous net contributions [*Richey et al.*, 2002].

[4] From a hydrological point of view, analysis of the flow, spatial distribution, and storage of fresh water on land is a key issue for understanding global water and energy cycles. For instance, river discharge represents one of the principal drivers of the ocean freshwater budget and contributes significantly to the variability in sea surface temperature and salinity [*Rango*, 1997; *Cao et al.*, 2002]. Floodplains and periodically inundated wetlands are also

[1]NOAA Cooperative Remote Sensing Science and Technology Center, City College of New York, New York, New York, USA.
[2]Laboratoire d'Etudes du Rayonnement et de la Matière en Astrophysique, CNRS, Observatoire de Paris, Paris, France.
[3]CNRS, Laboratoire de Météorologie Dynamique, Université Pierre et Marie Curie, Paris, France.
[4]NASA Goddard Institute for Space Studies, New York, New York, USA.


0148-0227/10/2009JD012674

critical for understanding hydrological processes [*Coe et al.*, 2002; *Decharme et al.*, 2008], as they regulate river hydrology due to storage effects along channel reaches [*Alsdorf et al.*, 2007a], modulate atmospheric temperatures, and contribute to increased evaporation [*Krinner*, 2003]. Finally, surface fresh waters are also important for water resource management [*Vörösmarty et al.*, 2000; *Gleick*, 2003] and biodiversity conservation [*IPCC*, 2007].

[5] There is now widespread recognition of the need for better observations and understanding of surface water distribution and variations globally [e.g., *Marburger and Bolten*, 2005; *United Nations*, 2004]. However, with approximately 60% of the world's floodplains and wetlands inundated during some portions of the year, our current knowledge of the spatial extent and variability of the land surface water cycle at the regional to global scales is still incomplete [*Finlayson et al.*, 1999].

[6] Our current knowledge of the spatiotemporal variations of continental waters relies on sparse in situ gauge measurements and partially verified hydrological models. In situ gauge measurements help quantify the movement of water (discharge) at a few points along river channels but provide comparatively little information on the spatial dynamics of surface water extent in floodplains and wetlands. In addition, the availability of ground-based gauge information has decreased dramatically during the last decade [*Alsdorf and Lettenmaier*, 2003], especially in remote areas like the Arctic [*Vörösmarty et al.*, 2001] and inaccessible tropical regions. For instance, the area centered on Manaus in the central Amazon basin includes only ~10 gauges, and the Rio Negro, with its 40,000 $m^3/s$ annual average flow, is almost completely ungauged [*Alsdorf et al.*, 2007a]. Even in places where stream gauges exist, legal and institutional restrictions often make the data unavailable for scientific purposes. Lacking spatially complete measurements of inundation/wetland locations, sizes, and water storage, hydrologic models have difficulties properly partitioning precipitation among these several components and represent their effects on river discharge at continental to global scales [*Alsdorf and Lettenmaier*, 2003]. Errors can exceed 100% because inundated surfaces modulate runoff by temporarily storing and changing runoff and evaporation [*Coe*, 2000; *Alsdorf et al.*, 2007a]. Partially verified hydrological models also have limits as far as predicting changes in the hydrology system under a warming climate. Our ability to measure, monitor, and forecast supplies of fresh water using in situ methods and hydrological models is facing considerable difficulties, at least at the global and continental scales.

[7] Over the last 20 years satellite remote sensing techniques have been very useful for large-scale hydrology investigations [*Smith*, 1997; *Alsdorf et al.*, 2003, 2007a; *Cazenave et al.*, 2004], as they provide a unique means to observe large regions continuously and are the only alternatives to in situ data in remote areas. Recent advances in remote sensing have demonstrated that some hydraulic variables can be measured reliably from satellites. For example, satellite altimetry (Topex/Poseidon (T/P), Jason-1, ERS, and Envisat missions) has been used for systematic monitoring of water levels of large rivers, lakes, and floodplains, now providing an ~15 year long time series [*Birkett*, 1998; *Birkett et al.*, 2002; *Gennero et al.*, 2005]. Since 2002 the Gravity Recovery and Climate Experiment (GRACE) gravity mission has provided direct estimates of the spatiotemporal variations in total terrestrial water storage for the first time (the sum of ground water, soil water, surface water, and snow pack) at seasonal and basin scales [*Tapley et al.*, 2004a, 2004b; *Ramillien et al.*, 2005, 2006; *Rodell et al.*, 2006].

[8] Surface water extent and its variations can also be measured with a variety of remote sensing techniques employing visible, infrared, or microwave observations [*Alsdorf et al.*, 2007a; *Prigent et al.*, 2007]. The following nonexhaustive list of techniques offers varying degrees of success regarding the diverse applications they are developed for. For instance, synthetic aperture radars (SARs) show very large capabilities to measure surface water extent. Studies in the Amazon basin [*Smith and Alsdorf*, 1998; *Hess et al.*, 2003; *Alsdorf et al.*, 2007b] or in the Congo prove the ability of SAR to delineate accurately the surface water in tropical forest environments with high spatial sampling intervals (~100 m). However, large data volumes have limited these studies to a few samples of a few basins, preventing systematic, long-term assessments of inundation dynamics. Estimations of surface water extent using visible or infrared measurements provide a high spatial resolution but show limitations for detecting surface water beneath clouds or dense vegetation. The potentials for using the Moderate Resolution Imaging Spectroradiometer (MODIS) to monitor temporal changes in flooding are, however, demonstrated over specific regions such as the Mekong River [*Sakamoto et al.*, 2007] and arid regions such as the Inner Niger Delta [*Berge-Nguyen et al.*, 2008]. Other active microwave instruments such as the dual-frequency T/P radar altimeter are also valuable for detecting inundations, but because of their narrow surface track, the estimation of water body extent is limited to polar regions where their polar orbit yields better spatial coverage [*Papa et al.*, 2006a]. Passive microwave observations have long been shown to detect surface water extents [*Gidding and Choudhury*, 1989]. However, most studies have been dedicated to specific areas like the Amazon basin [*Sippel et al.*, 1998] or Arctic regions [*Mialon et al.*, 2005]. In addition, the microwave signal can be contaminated by the atmosphere (water vapor), clouds, and rain, modulated by surface temperature, or altered by the presence of vegetation in mixed open water/vegetation scenes. These factors can distort time series estimates of surface water variations. These considerations lead to the conclusion that there is not a unique and exclusive technique for detecting open water regardless of the environment. A multisatellite technique is needed for the retrieval of surface water extent and dynamics at the global scale. Combining observations from different instruments makes it possible to capitalize on their complementary strengths, to extract maximum information about inundation characteristics, and to minimize problems related to analysis of measurements by one instrument only [*Prigent et al.*, 2001a].

[9] In this context a globally applicable remote-sensing technique employing a suite of complementary satellite observations has been developed to estimate spatial and temporal dynamics of surface water extent. This data set has been generated from several satellite instrument types: passive microwave, active microwave, and visible and near-

IR imagery. The first results were obtained for 1 year [*Prigent et al.*, 2001a]. *Prigent et al.* [2007] presented results over 8 years (1993–2000), and monthly results of spatial and temporal dynamics of inundations were analyzed and evaluated for different environments by comparison with in situ measurements and other related remote sensing observations. Compared with different independent static data sets, each representing subsets of the inundation extent from the multisatellite technique (including the wetlands distribution from *Matthews and Fung* [1987], the rice paddies distribution from *Matthews et al.* [1991], and the inland permanent water from the International Geosphere-Biosphere Programme (IGBP) [*Loveland et al.*, 2000]), the results showed very realistic global distributions for all latitudes and environments, with, however, a limitation of the multisatellite approach in detecting most small inland water bodies that cover less than 10% of a pixel (a pixel covers 773 km$^2$).

[10] The method was also carefully studied over the Indian subcontinent for 2 years [*Papa et al.*, 2006b] and over boreal environments during 8 years [*Papa et al.*, 2007, 2008a]. This data set has also been used recently for climatological and hydrological analyses, such as evaluation of methane surface emission models [*Bousquet et al.*, 2006; *Ringeval et al.*, 2010], validation of the river flooding scheme in land surface models [*Decharme et al.*, 2008], and estimation of water volume changes in the Rio Negro by combining surface water extent and altimetry-derived level height [*Frappart et al.*, 2008, *Papa et al.*, 2008b]. *Papa et al.* [2007] evaluated the consistency of spatial and temporal variations of this inundation data set over the Ob River basin using in situ snow depth and river runoff, and *Papa et al.* [2008a] investigated the response of river discharge to seasonal flood change in the large Siberian watersheds.

[11] The objective of this study is to present the global surface water extent data set extended to 12 years, 1993–2004. The ERS scatterometer encountered serious technical problems after 2000 and the processing scheme had to be adapted. The adjustment of the methodology, the various options, and their evaluations over 8 years are discussed in section 2, together with the introduction of a newly fine-tuned mixing model. Section 2 also deals with the extension of the global emissivity data set to 1993–2004 and the adjustments done to overcome an artifact in ancillary data. In section 3 the global results for the surface water extent are presented over the 1993–2004 period. A comparison with the Global Lakes and Wetlands Database (GLWD) of *Lehner and Doll* [2004] is performed. Section 4 deals with assessment of the new data set versus other independent observations at the global scale, for large inland surface water bodies and large river basins. Finally, conclusions and perspectives are discussed in section 5.

## 2. Extension of the Global Surface Water Extent Data Set

### 2.1. Initial Methodology and the Original 8 Year Data Set

[12] The methodology that captures the surface water extent, comprising episodic and seasonal inundations, wetlands, rivers, lakes, and irrigated agriculture at the global scale is described in detail by *Prigent et al.* [2007]. The complementary suite of satellite observations used to detect and quantify surface water extent covers a large wavelength range.

[13] (a) Passive microwave emissivities between 19 and 85 GHz: These are estimated from the Special Sensor Microwave/Imager (SSM/I) observations by removing contributions of the atmosphere (water vapor, clouds, rain) and modulation by the surface temperature, using ancillary data from visible and IR satellite observations from the International Satellite Cloud Climatology Project (ISCCP) [*Rossow and Schiffer*, 1999] and the National Center for Environment Prediction (NCEP) reanalysis [*Kalnay et al.*, 1996].

[14] (b) ERS scatterometer backscatter at 5.25 GHz (5.71 cm; active microwave): Because ERS measurements are performed at different incidence angles and the repeat cycle is not short enough to provide multiple observations of the same scene with a single incidence angle during a month, a linear interpolation is applied to all incidence angles between 25° and 50° for a month and the interpolated value at 45° is used.

[15] (c) Advanced very high resolution radiometer (AVHRR) visible (0.58–0.68 $\mu$m) and near-IR (0.73–1.1 $\mu$m) reflectances and the derived normalized difference vegetation index (NDVI) from the 8 km product generated under the joint NOAA and NASA Earth Observing System pathfinder project [*James and Kalluri*, 1994].

[16] A full description of each satellite observation is given by *Prigent et al.* [2001b].

[17] Passive microwave emissivities are particularly sensitive to the presence of open water. The NDVI information is very important for discriminating between arid surfaces and surface waters, which can have rather similar microwave emissivities. Active microwave information plays a key role in the estimation of the vegetation scattering contribution within an inundated pixel. The methodology can be summarized as follows. All remote sensing data are averaged over each month on an equal-area grid of 0.25° at the equator (a pixel covers 773 km$^2$). An unsupervised classification of the three sources of satellite data is performed and pixels with satellite signatures likely related to surface water are retained. For each inundated pixel the monthly fractional coverage by open water is obtained using the passive microwave signal and a linear mixture model with end members calibrated with scatterometer observations to account for the effects of vegetation cover [*Prigent et al.*, 2001a]. As the microwave measurements are also sensitive to snow cover, snow masks are used to edit the results and avoid any confusion with snow-covered pixels. The weekly North Hemisphere and South Hemisphere snow mask from the National Snow and Ice Data Center (University of Colorado; NSIDC) is adopted and averaged on a monthly basis [*Armstrong and Brodzik*, 2005]. The technique is globally applicable without any calibration for individual environments [*Prigent et al.*, 2007]. Note that inland seas (Caspian Sea, Aral Sea), large lakes such as the Great Lakes in North America, for instance, and coastal pixels that are likely contaminated by the ocean are suppressed from the results [*Prigent et al.*, 2007], using the IGBP 1-min land ecosystem classification map [*Loveland et al.*, 2000].

**Table 1.** Summary of the Six Cases of Global Surface Water Extent Produced for 1993–2000[a]

| Case | SSM/I | ERS | AVHRR/NDVI | Mixture Model |
|---|---|---|---|---|
| 1 | TV | TV | TV | Old |
| 2 | TV | TV | TV | New |
| 3 | TV | C | C | Old |
| 4 | TV | C | C | New |
| 5 | TV | TV | C | Old |
| 6 | TV | C | TV | Old |

[a]AVHRR, advanced very high-resolution radiometer; C, monthly climatology derived from 8-year monthly time series (1993–2000); NDVI, normalized difference vegetation index; SSM/I, Special Sensor Microwave/Imager; TV, time-varying. Case 1 is the "original estimates" [*Prigent et al.*, 2007], and case 4 is the "new estimates" (this study).

## 2.2. Issues and Options for Data Set Extension

### 2.2.1. The ERS and Normalized Difference Vegetation Index Limitations

[18] The use of active microwave observations in the estimation of surface water extent is important because it helps identify inundated pixels and is used in the linear mixture model to account for the effects of vegetation cover. After 2000 the ERS satellite suffered several difficulties, which is why our first analysis ended there. In January 2001 the ERS lost its gyroscopes, causing the yaw to vary between $+2^{o}$ and $-2°$. This problem was fixed in August 2003, with the installation of a new processor, but in June of the same year the satellite lost its onboard recording capability, and since then it relies on the voluntary support of ground stations. With the ERS being essentially dedicated to ocean research, acquisition of ocean data is a priority, so there is very limited storage of land observations after 2000.

[19] To overcome the lack of the ERS scatterometer data after 2000, we first investigated the possible use of observations from the SeaWinds scatterometer on board QuikSCAT, launched in 1999. SeaWinds observes in the Ku band (13.4 GHz) at 45° and 54° incidence angles in horizontal/horizontal (HH) and vertical/vertical (VV) polarizations, respectively, whereas the ERS scatterometer provides measurements in the C band (5.25 GHz) in VV polarization for viewing angles from 18° to 59°. During 2000 both satellites delivered quality observations. Comparisons of the two scatterometer observations over continental surfaces showed that, due to the frequency and polarization differences, it was not possible to mimic the ERS observations with the SeaWinds ones, especially over vegetated water surfaces. Comparing the T/P altimeter backscattering coefficients in C (5.3 GHz) and Ku (13.6 GHz) bands over continental surfaces, *Papa et al.* [2002, 2003] reached a similar conclusion: the sensitivity of the backscattering to vegetation and roughness is strongly frequency dependent. Using the SeaWinds scatterometer data instead of the ERS observations in our analysis would require a complete retuning of the methodology, which might still cause a discontinuity in the time series of the surface water extent. Another alternative is to use a monthly mean climatology of the ERS observations for the period 1993–2000. This option and the results are discussed in section 2.2.3.

[20] In addition to the ERS difficulties after 2000, the consistency of a NDVI data set over a long time period is in doubt. NDVI calculations from the AVHRR record are sensitive to the instrument intercalibration of the various NOAA satellites over time, as well as to sensor degradation and satellite drift [*Cracknell*, 1997; *Gutman*, 1999; *Tucker et al.*, 2005]. For instance, a significant jump in the NDVI was observed at the end of 1999 in the NOAA/NASA pathfinder data set, corresponding to the switch from NOAA-14 to NOAA-16: these two AVHRR instruments were built by two different manufacturers. To avoid introducing spurious variations in our surface water extent data set from the NDVI record over the 1993–2004 period, use of a monthly mean climatology of NDVI is also tested (section 2.2.3).

### 2.2.2. Use of a New Mixing Model

[21] The former version of the model tended to overestimate the fraction of inundations for large flooded areas and underestimate the fraction of inundations for areas with low inundations (see the comparison of the surface water data set with the SAR estimates given by *Prigent et al.* [2007]). As a consequence, we also decided to tune the linear mixing model used in the methodology that relies on the statistical relationship between the SSM/I polarization difference at 37 GHz and the ERS backscatter (see Figure 2 of *Prigent et al.* [2001a] for the scatterplot between the two variables).

### 2.2.3. Comparison of the Different Data Options Over 1993–2000

[22] To evaluate the use of ERS and AVHRR climatologies and the new linear mixing model, monthly multisatellite surface water extent estimates have been produced at the global scale for 1993–2000 in six different ways using the following data.

[23] 1. Time-varying SSM/I, ERS, and AVHRR data with the old linear mixing model (original results as described previously here and discussed by *Prigent et al.* [2007]), called case 1.

[24] 2. Time-varying SSM/I, ERS, and AVHRR with the new mixing model, called case 2.

[25] 3. Time-varying SSM/I with the ERS and AVHRR climatologies and the old model, called case 3.

[26] 4. Time-varying SSM/I data with the ERS and AVHRR climatologies and the new model (also called the "new estimates"), called case 4.

[27] 5. Time-varying SSM/I and ERS data with the AVHRR climatology and the old linear mixing model, called case 5.

[28] 6. Time-varying SSM/I and AVHRR data with the ERS climatology and the old linear mixing model called case 6.

[29] Table 1 summarizes the six cases. The latter two estimates (case 5 and 6) will help interpret the results and the differences observed for each instrument when using a climatology or the time-varying signal (solutions with only one climatology and the new linear mixing model are not shown).

[30] Figure 1 compares the results from the six versions and shows the seasonal and interannual variations (left) and the associated anomalies (right; computed by subtracting the monthly mean over 1993–2000 from the monthly time series) of the surface water extent globally and in three latitude zones over the period 1993–2000. The original estimates as in *Prigent et al.* [2007] (case 1, the original estimates; red lines); the new estimates, which use both AVHRR and ERS climatologies and the new model (case 4; black lines with filled circles); case 2 (blue lines); and case 3

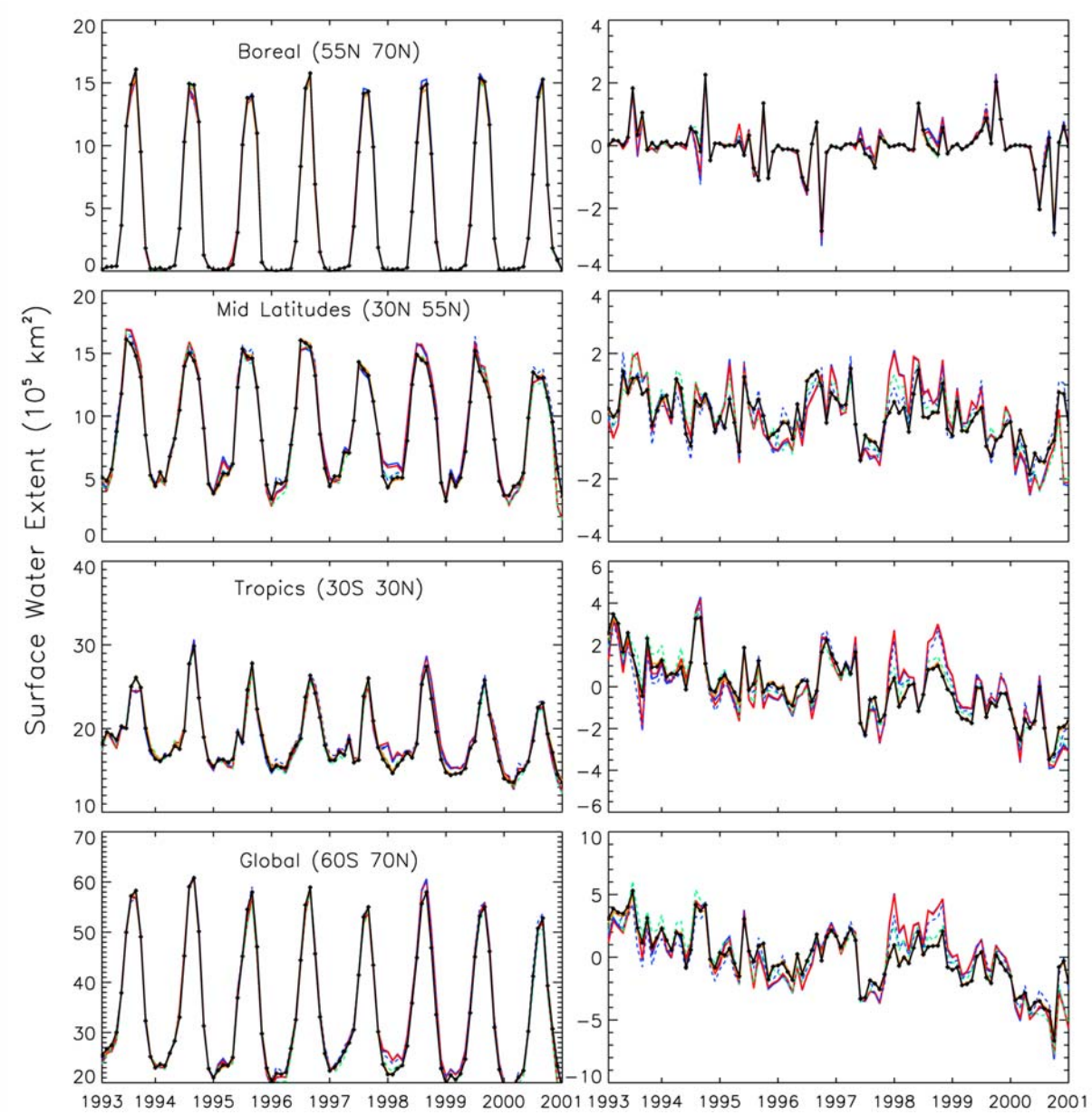


**Figure 1.** Seasonal variations (left) and associated anomalies (right; obtained by subtracting the 12 year mean monthly value from individual months) of the surface water extent globally and for three latitude zones over the period 1993–2000: original estimates as in *Prigent et al.* [2007] (case 1; red lines), new estimates (case 4; black lines with filled circles), case 2 (blue line), case 3 (yellow line), case 5 (dashed blue line), and case 6 (dashed green line). The different cases are summarized in Table 1.

(yellow lines). The estimates with one climatology only and the old model are represented by the dashed blue lines (case 5) and with dashed green lines (case 6). The left side in Figure 1 clearly shows that the six estimates over the 8 years have the same general behavior, with similar seasonal and interannual variations at the global scale and for the different latitude bands. The six data sets are highly correlated (>0.98), with the largest differences at the minimum or maximum of the extent, regardless of the latitude. In addition to Figure 1, Table 2 summarizes the statistics regarding case 1 (mean, mean maximum, and mean minimum over the record) and the differences between case 1 and the five other cases for the midlatitudes, the tropics, and the global scale. For boreal regions, as shown in Figure 1, the differences were extremely small and we decided not to report the values in Table 2. Table 2 shows that the differences between case 1 and the other cases are, in general, of the order of a few percent and, most of the time, below 2%, regardless of the latitude band. The three largest differences are noted in the midlatitude band for the mean minimum values between case 1 and cases 3–5. The differences between case 1 (original estimates) and case 4 (the new estimates) are generally small, less than 1% at the global scale for the mean, maximum, and minimum.

[31] The six anomaly signals (Figure 1, right) are also in good agreement, showing that the average total surface

**Table 2.** Surface Water Extent: Statistics for the Six Cases Related to Figure 1

| | Midlatitudes | | | Tropics | | | Global | | |
|---|---|---|---|---|---|---|---|---|---|
| | Mean | Max. | Min. | Mean | Max. | Min. | Mean. | Max. | Min. |
| Case 1 | 906,000 | $1.53 \times 10^6$ | 354,000 | $1.90 \times 10^6$ | $2.63 \times 10^6$ | $1.52 \times 10^6$ | $3.42 \times 10^6$ | $5.69 \times 10^6$ | $2.05 \times 10^6$ |
| Case 1–case 2 | −3300 | 6,200 | −10,200 | 14,900 | −7300 | 26,300 | −500 | −27,100 | 13,500 |
| | (−0.36) | (0.41) | (−2.88) | (0.78) | (−0.28) | (1.73) | (−0.01) | (−0.47) | (0.17) |
| Case 1–case 3 | 14,000 | 18,700 | −21,900 | 700 | −16,100 | −7,600 | 19,300 | 240 | −27,400 |
| | (1.52) | (1.22) | (−6.1) | (0.36) | (0.61) | (−0.50) | (0.56) | (0.004) | (0.004) |
| Case 1–case 4 | 12,300 | 24,700 | −12,400 | 17,000 | −20,200 | 21,200 | 23,000 | −21,000 | −8,400 |
| | (1.36) | (1.61) | (−3.50) | (0.89) | (−0.77) | (1.39) | (0.67) | (−0.36) | (−0.11) |
| Case 1–case 5 | −12,600 | −13,700 | −14,400 | −29,200 | −41,100 | −26,300 | −49,300 | −58,900 | −76,100 |
| | (−1.39) | (−0.89) | (−4.09) | (−1.53) | (−1.56) | (−1.73) | (−1.44) | (−1.03) | (−0.98) |
| Case 1–case 6 | 28,100 | 34,100 | 10,400 | 34,900 | 35,100 | 27,400 | 75,800 | 69,700 | 40600 |
| | (3.1) | (2.22) | (2.93) | (1.83) | (1.33) | (1.80) | (2.21) | (1.22) | (0.52) |

[a]The 8-year mean, 8-year mean maximum, and 8-year mean minimum for 1993–2000 from the original estimates (case 1; $km^2$) for the midlatitudes, and the tropics and at the global scale and the difference ($km^2$) between case 1 and the other five cases. The value in parentheses represents the difference (%) compared to case 1 estimates. The different cases are summarized in Table 1.

water extent is not changed significantly by the introduction of the new mixture model. The surface water extent for each latitude band using the old and new linear models is similar. The anomalies reveal that small differences are, however, introduced by the use of the climatologies. The differences are larger during years that are affected by special events such as the strong El Niño in 1998, in regions where this phenomenon has a significant impact. The magnitude of the anomaly for the estimates using both climatologies (cases 3 and 4) is lower than the original estimates (case 1) or the estimates using only one climatology (case 5 and 6), as expected: part of the interannual variability in the original data set is related to the variability in the ERS and AVHRR signals, and when the climatologies are used, this variability is partially removed. The major differences between the new estimates (case 4) and the original calculation (case 1) occur in January 1998 over midlatitudes (~140,000 $km^2$ difference; 26% of the total surface water extent over midlatitudes) and in August 1998 over the tropics (~150,000 $km^2$; 6% of the total surface water extent over the tropics). Note that the estimates using both climatologies (case 3 and 4) are always closer to the one using the ERS climatology only (case 6), whereas the original estimates (case 1) are always closer to those using the NDVI climatology only (case 5): the observed differences between the new and the original data sets are thus mainly due to the ERS signal, which is used both in the detection of the inundated pixel and in the estimates of the fractional surface water extent within the pixel.

[32] For a closer look at the difference introduced in the estimates using or not using the climatologies and the old and new linear mixing models, maps over the Indian subcontinent are displayed in Figure 2, for a month with large differences (August 1998). We chose the Indian region, because the original data set was extensively evaluated over this area by *Papa et al.* [2006b]. Figure 2 displays the surface water extent from the new estimates (case 4; Figure 2a), the difference between the new estimates and the original estimates (case 4 − case 1; Figure 2b), the difference for the new estimates minus the estimates using time-varying ERS/AVHRR and the new model (case 4 − case 2; Figure 2c). Figure 2d shows the difference between the new estimates and those using climatologies and the old model (case 4 − case 3), together with the histograms of the surface water extent over the region for cases 4 and 3.

[33] In general, Figure 2 confirms that the differences between the new estimates and the other cases are limited even during a month of maximum discrepancies (absolute differences <20 $km^2$ per pixel are not displayed). In Figures 2b (case 4 − case 1), 2c (case 4 − case 2), and 2d (case 4 − case 3), only a few areas show differences larger than 60 $km^2$ per pixel (i.e., >8% of the pixel surface). When looking at case 4 − case 1 (Figure 2b), the new estimates shows larger values ~20–60 $km^2$ per pixel in eastern India, in the center plains of the Ganges, and over the Indus River and lower values in central India, with a difference of ~20–40 $km^2$. Most of the time the differences are lower than ~10% of the surface water extent values. When analyzing the difference (case 4 − case 2) introduced by the climatologies only (with the new linear mixing model) as in Figure 2c, we also checked the ERS observations for that specific month and compared it with the ERS monthly climatology: this confirmed that the differences in surface water extent were closely related to the differences in ERS observations. When looking at the effects introduced by the use of the old or new model only with both climatologies (case 4 − case 3) as in Figure 2d, it is clearly shown that, overall, the differences are always lower than ~10%–15% of the surface water extent estimates. To show the effect of the new mixture model compared to its previous version, two histograms, for cases 3 and 4, are also displayed. The improvement of the mixture model was made using the comparison between the multisatellite approach estimates and the high-resolution SAR images over the Amazon River [*Prigent et al.*, 2007]. This comparison shows that the first version of the mixture model tended to overestimate the fraction of inundations for large flooded areas and to underestimate the fraction of inundations for areas with low inundations. Over India, case 3 (old model) shows, for instance, a significant jump in the distribution of surface water extent at the end of the histogram, with more than 175 pixels detected as totally flooded. The use of the new mixture model (case 4) helped correct this artifact and shows a more realistic distribution for pixels with an inundation area >650 $km^2$, the total number of totally flooded pixels now being 54. The comparison of the two histograms also shows that the new mixture model helps

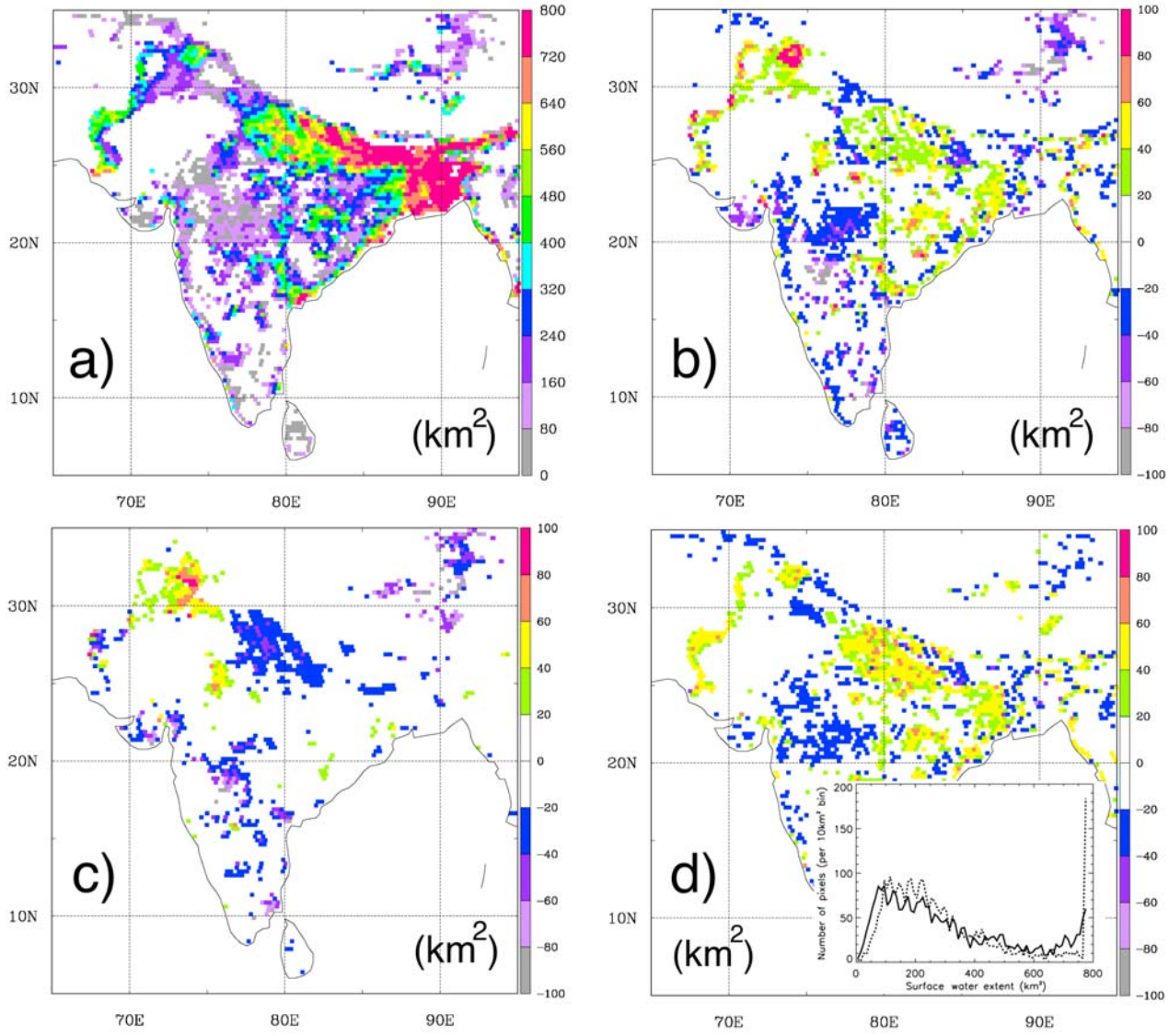


**Figure 2.** Maps over the Indian subcontinent for August 1998 (km$^2$): (a) surface water extent for August 1998 from the "new estimates" (case 4); (b) map of the difference, case 4 − case 1; (c) map of the difference, case 4 − case 2; (d) map of the difference, case 4 − case 3. Inset in Figure 2d: histograms of surface water extent estimates for cases 3 and 4. The different cases are summarized in Table 1.

to increase the number of pixels with inundation areas ~80 km$^2$. However, as already demonstrated by *Prigent et al.* [2007], the radiometer and the retrieval algorithm are not sensitive enough to detect most inland water bodies that cover less than ~80 km$^2$ within a pixel and probably still underestimate the small surface water, comprising less than 10% of the fractional coverage of equal-area grid cells.

[34] To summarize, Figure 3 shows the histogram of the differences for the new estimates minus the original ones from *Prigent et al.* [2007] (case 4 − case 1). The histogram is constructed at the global scale and for the 8 years 1993–2000 for the pixels detected as flooded only. It clearly shows that most of the differences between the two data sets range between −25 and 25 km$^2$ (<3.5% of a pixel).

[35] We are aware that the introduction of the climatologies in the methodology can have spurious effects for specific events (such as the one illustrated in Figure 2). We keep this limitation in mind for further analysis, but for most applications it does not affect the conclusions. The data set can then be extended with good confidence beyond 2000, using the ERS and AVHRR climatologies and the new mixture model.

[36] Moreover, the good performance using a climatology rather than coincident vegetation information will be the basis for future development of the data set at a better time-sampling interval. Indeed, this new result clearly suggests that the vegetation-related portions of the microwave signal generally vary more slowly than the water-related portion so that the time interval of the results can be reduced in the future from 1 month to 5 days, and possibly 1 day, by applying the existing technique to individual orbit swaths of SSM/I data.

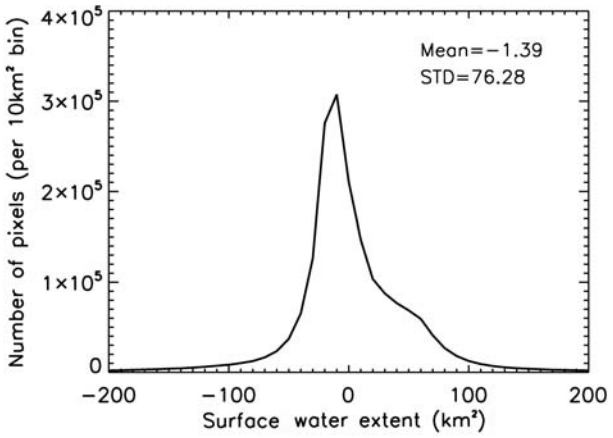


**Figure 3.** Histogram of the difference between the "new estimates" and the "original estimates" (case 4 − case1) at the global scale and for 8 years (1993–2000). Only pixels classified as inundated are taking into account.

### 2.3. Global Emissivity Data Set, 1993–2004

[37] Passive microwave emissivities between 19 and 85 GHz estimated from the SSM/I observations are the core data set used in our methodology to estimate global surface water extent. First available from 1993 to 2000, the emissivity time series have been extended to 2004 following the methodology described by *Prigent et al.* [1997, 2006]. However, intensive analyses of the emissivity times series recently revealed an issue after September 2001, as illustrated in Figure 4. Figure 4a shows the times series for the emissivities at 37 GHz in horizontal polarization (H) for the globe (continental surfaces only) and two selected regions. At the global scale there is clearly an abrupt change in the emissivities after September 2001, with a sharp decrease of about 0.012. Over selected areas this artifact shows large variations from region to region. A similar abrupt change is observed for the emissivities spatially averaged over the Nile River basin, whereas the time record over the Amazon River basin shows almost no change throughout the record. A similar test was performed for the emissivities at 19 and 37 GHz at V polarization, and similar behaviors were observed in September 2001.

[38] The cause of this discrepancy in the emissivity data sets has its main source in the abrupt change from September 2001 observed in the ISCCP surface skin temperature derived from IR observations [*Rossow and Schiffer*, 1999] that are used in the emissivity calculation methodology [see equations 1 and 2 and Figure 1 in *Prigent et al.*, 2006]. This is illustrated in Figure 4b, which shows the change in the monthly mean surface skin temperature from ISCCP after September 2001 at the global scale, for the Nile and the Amazon rivers. In October 2001 the NOAA operational sounder analysis, which produces the TIROS Operational Vertical Sounder (TOVS) atmospheric temperature and humidity profile products used in the ISCCP analysis, was changed to a new method [*Zhang et al.*, 2006]. This change introduced a sudden and systematic change in the temperature and water vapor in the atmosphere, causing a systematic increase in retrieved surface temperatures. This leads to a difference of about 2 K in the global mean surface temperatures calculated from January 1993 to September 2001 versus from October 2001 to 2004. This difference is, however, less than 1% of the global mean surface temperature of ~289 K over the record and still within the error estimates for surface temperature retrievals.

[39] To illustrate at the global scale the impacts of the offset in surface skin temperatures on the emissivities themselves (we show here the emissivities at 37 GHz H polarization), Figure 5 displays, for each parameter, maps of the difference in their means for the period 1993–2001 and 2001–2004 during summer (June, July, and August; JJA). Figure 5a shows that the difference in surface temperature is not uniform over the globe with large geographical features. Large negative values, up to more than −6 K, are mainly found in a band from eastern Africa to northern Eurasia and in the western United States, whereas large positive values, up to more than +6 K, are found in northern Canada and eastern Eurasia. The impacts on microwave emissivities related to the offset in surface skin temperatures are shown

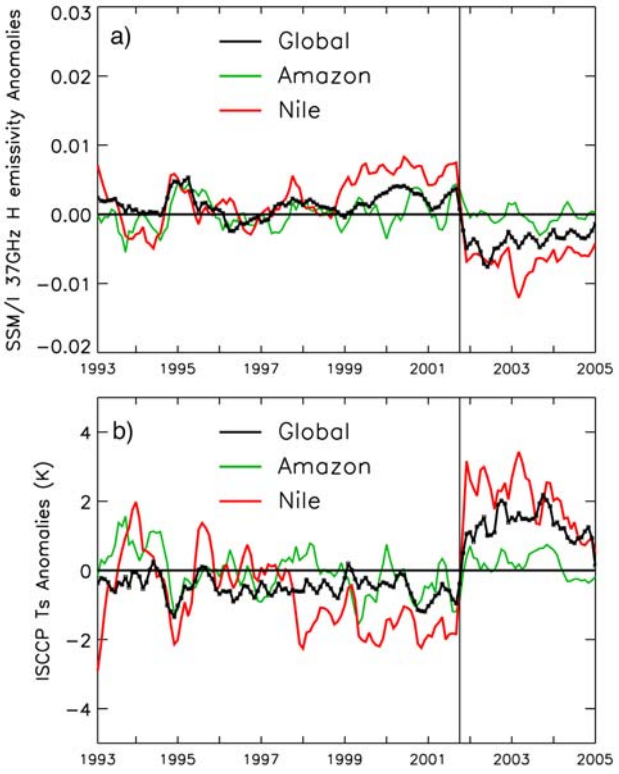


**Figure 4.** (a) Time series of deseasonalized anomalies (obtained by subtracting the 12-year mean monthly value from individual months) of monthly mean Special Sensor Microwave/Imager (SSM/I) 37 GHz horizontal (H) polarization emissivity for the period 1993–2004. The black line represents the emissivity spatially averaged over the globe (continental surfaces), the red line is over the Nile basin, and the green line is over the Amazon basin. (b) Same as Figure 4a but for the International Satellite Cloud Climatology Project (ISCCP) surface skin temperature ($T_s$) derived from IR observations. A moving average of ±1 month is applied to all curves.

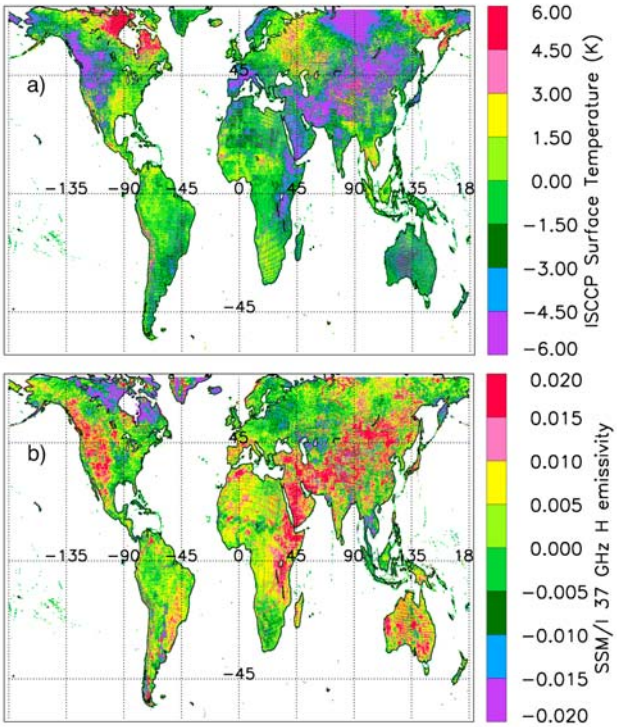


**Figure 5.** (a) ISCCP IR-derived surface skin temperature difference between June–July–August (JJA) 1993–2001 and JJA 2001–2004. (b) Difference in SSM/I 37 GHz H polarization emissivity between JJA 1993–2001 and in JJA 2001–2004.

in Figure 5b, where there is a large band of high positive values from eastern Africa to northern Eurasia and in the western United States, whereas northern Canada shows large negative values.

[40] To correct the artifact, we decided to work directly on the monthly mean emissivity data set for each channel and polarization. After several tests we decided to correct them by adjusting the two subseries January 1993–September 2001 and October 2001–December 2004 locally for each month. For each frequency, each polarization, and each pixel, the mean values for all January 1993–2001 and all January 2002–2004 are calculated and the difference is removed by adjusting the 2002–2004 time series to the 1993–2001 series. This is done for each month of the year, considering the 1993–2000 and 2001–2004 times series from the month of October. Figure 6 shows the times series for the emissivities at 37 GHz in H polarization for the globe, the Nile River, and the Amazon River after the correction is applied and the artifact is removed.

[41] Using the corrected data sets of emissivities, the ERS and AVHRR climatologies, and the new mixture model, we can now extend the global data set of surface water extent for the period 1993–2004.

## 3. The 12 Year Global Surface Water Extent Data Set

[42] Estimates of global monthly mean surface water extent have been produced for 1993–2004 using the new methodology described in section 2.2 and the 1993–2004 global emissivity data set corrected as described in section 2.3. Figure 7 shows the annual maximum surface water extent averaged over the 12 years, regardless of month of maximum. At the global scale the results exhibit very realistic distributions, with major inundated areas well captured for all latitudes and environments. Inundation associated with major river systems is well delineated, even in complex regions characterized by extensive flooding below dense vegetation canopies such as the Amazon and Congo rivers. Seasonal wetlands, such as the Pantanal in South America and the Okavango Delta in Botswana, are also realistically captured. Irrigated agriculture, such as rice crops, exhibits a strong signature in Southeast Asia and large floodings are observed in the Ganges-Brahmaputra River system and its delta in Bangladesh. In northern regions large inundated areas in Canada are consistent with the presence of small lakes and the inundated areas around the Ob, the Yenisey, and the Lena tivers in Siberia are also well reproduced and have been intensively assessed by *Papa et al.* [2006a, 2007, 2008a].

[43] *Prigent et al.* [2007] compared the results over 1993–2000 with different independent static data sets, including the wetlands distribution of *Matthews and Fung* [1987], the rice paddy distribution of *Matthews et al.* [1991], and the inland permanent water from IGBP [*Loveland et al.*, 2000]. Given that the multisatellite method does not discriminate among inundated wetlands, coastal wetlands, rivers, small lakes, irrigated agriculture, and floodplains, each of these data sets represented a subset of the satellite-derived inundation extent. The GLWD of *Lehner and Doll* [2004] represents a more comprehensive data set of global surface water area, including small and large lakes, reservoirs, smaller water bodies, and rivers, and a good representation of the maximum global wetland extent. Figure 7 also shows the comparison between the latitudinal distribution of surface water derived from the multisatellite technique and that

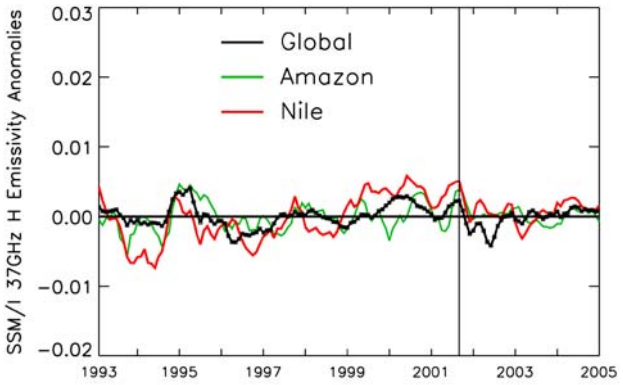


**Figure 6.** Time series of deseasonalized anomalies (obtained by subtracting the 12-year mean monthly value from individual months) for the period 1993–2004 of monthly mean SSM/I 37 GHz H polarization emissivity after removing the artifact from October 2001. The black line represents the emissivity spatially averaged over the globe (continental surfaces), the red line is over the Nile basin, and the green line is over the Amazon basin. A moving average of ±1 month is applied to all curves.

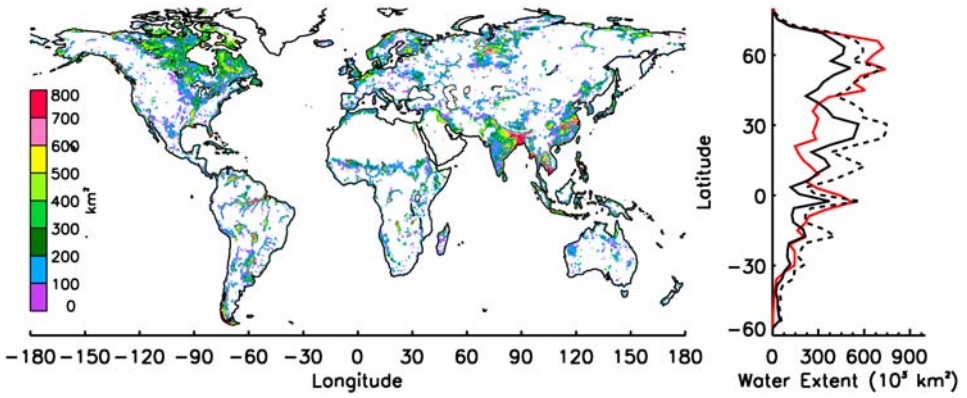


**Figure 7.** Global map of the annual maximum surface water extent (averaged over 1993–2004) derived from the multisatellite method. The spatial resolution is 773 km$^2$ (i.e., equal-area grid of 0.25° × 0.25° at the equator). Also shown are the latitudinal distributions of global surface water for three estimates: the annual maximum surface water extent averaged over 1993–2004 (as shown on the map; solid black line); the maximum surface water extent reached for each pixel over 1993–2004 (dashed black line); and the surface water extent from the Global Lakes and Wetlands Database (GLWD; level 3; red line) of *Lehner and Doll* [2004]. Surface water extent values are aggregated in steps of 3°.

derived from the global static map (spatial resolution of 30 s) of lakes and wetlands (including reservoirs and rivers) from level 3 of the GLWD. Two different distributions are estimated from the multisatellite surface water data set: the distribution using the annual maximum surface water extent averaged over the 12 years (as for the map) and the distribution considering the maximum value for each pixel over the 12 year record. In general, the latitudinal distributions of global surface water from the satellite technique largely parallel the distribution from the GLWD. The total global surface water area from the GLWD covers about 12.8 × 10$^6$ km$^2$, while the total satellite-derived surface water covers about 10.1 × 10$^6$ km$^2$ taking the 12 year mean maximum and reaches 16.4 × 10$^6$ km$^2$ considering the maximum over the record. The two independent data sets agree exceptionally well for latitudes ranging from 40°N to 80°N and below 15°N. For these regions the distribution derived with the maximum over the record has an overall magnitude of surface water extent close to the values from the GLWD. For instance, for the band from 40°N to 80°N, the surface water area from the GLWD is ~6.4 × 10$^6$ km$^2$, while the satellite-derived area covers ~6.0 × 10$^6$ km$^2$. The major difference between the two data sets is found for the regions situated in the latitude band between 10°N and 30°N, where both satellite-derived surface water distributions significantly exceed the values from the GLWD. While the GLWD-3 covers ~1.9 × 10$^6$ km$^2$ in this latitude band, the extent of surface water from the satellite technique is more than doubled, with a maximum over the record of ~4.7 × 10$^6$ and ~3.1 × 10$^6$ km$^2$ using the 12 year mean maximum. This difference can be explained in part by the fact that GLWD-3 does not include the surface water area from irrigated agriculture and might underestimate the actual total surface water extent in these regions. As shown on the map, some regions in Asia and Southeast Asia show large areas of highly inundated surface, especially in India, along the Ganges-Brahmaputra River, and in eastern China, where rice dominates the agricultural landscape. These patterns are in good agreement with those observed on the Digital Global Map of Irrigation Area of *Siebert et al.* [2006]. *Siebert et al.* [2006] estimate that, on the country level, irrigated surfaces cover, for example, ~570,000 km$^2$ in India and ~540,000 km$^2$ in China. These values already explain a large part of the difference observed between the multisatellite approach and the GLWD in this latitude band. Another potential explanation of this difference is that the multisatellite method might encounter some difficulties in these regions in accurately discriminating between very saturated moist soil and standing open water.

[44] Seasonal and interannual variations of the total surface water extent and the associated anomalies are presented in Figure 8, globally (90°S–90°N) and for three latitude zones: the northern regions (30°N–90°N), the tropics (30°S–30°N), and the southern regions (90°S–30°S). Results show a strong seasonal cycle (Figure 8a), with a mean annual averaged maximum of 5.88 × 10$^6$ km$^2$ for 1993–2004. *Prigent et al.* [2007] (Figure 5, section 3.1) have discussed the agreement with several global or regional surveys representing various components of wetland and open-water distributions [*Matthews and Fung*, 1987; *Matthews et al.*, 1991; *Loveland et al.*, 2000; *Cogley*, 2003]. The extent shows a substantial interannual variability at large scales, globally, and in each latitude band, especially near the minima and maxima. At the global scale the maximum surface water extent varies from ~6.29 × 10$^6$ km$^2$ in July–August 1994 to ~5.46 × 10$^6$ km$^2$ in August 2000, and the minimum varies from ~1.87 × 10$^6$ km$^2$ in January 2000 to 2.31 × 10$^6$ km$^2$ in January 1993. The years 1994, 1996, 1998, and 2002 exhibit larger peaks. For 1994, 1998, and 2002, the peak appears mostly in tropical areas associated with the 1993/1994, 1997/1998, and 2002/2003 El Nino events (shaded in Figure 8a), whereas the 1996 peak appears mostly in northern latitude regions.

[45] Time series anomalies, computed by subtracting the mean monthly value from the monthly time series (Figure 8b), also reveal a slight overall reduction in the global inundated area between 1993 and 2004, but with large variations and changes over the record. The global

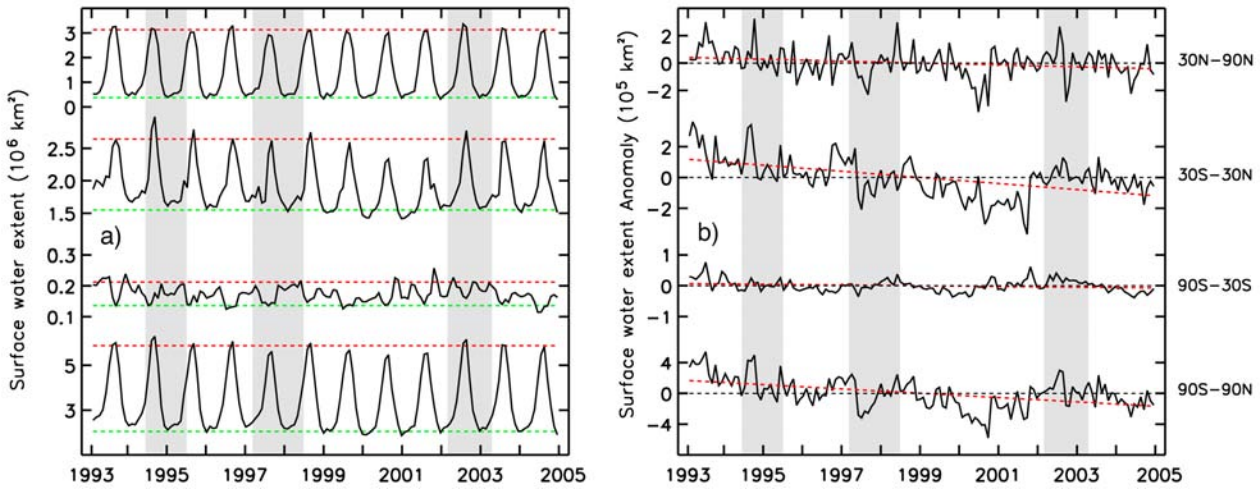


**Figure 8.** Monthly mean surface water extents and their anomalies for the period 1993–2004. (a) The black line is the monthly mean land surface water extent for 1993–2004 for the globe (bottom curve) and for three latitudinal regions (from bottom to top, 90°S–30°S, 30°S–30°N, and 30°N–90°N). The dashed red line is the 12-year mean maximum and the dashed green line is the 12-year mean minimum for 1993–2004. (b) Deseasonalized anomalies (obtained by subtracting the 12-year mean monthly value from individual months) for the same three latitudinal regions. The dashed red line is the linear fit. The shading indicates El Niño events.

surface water extent decreases significantly from 1993 to 2000, with a higher rate from 1998 to mid-2000. For the global record, the decrease in the surface water extent is about −27,700 km$^2$/year, that is, ~33,2400 km$^2$ between 1993 and 2004 ($R = -0.47$, $p$-value < 0.01 for $|R| > 0.21$; 144 points are used to compute the linear correlation coefficient $R$), representing an ~5.7% reduction of the mean annual maximum in 12 years. For the different latitude bands, the decrease is located mostly in the tropics. A linear fit gives a decrease of about −19,600 km$^2$/year for the tropical band ($R = -0.51$), representing an ~8.9% reduction in the mean annual maximum in 12 years. At the global scale and for the tropics, we note that the reduction in surface water extent happened mainly in the 1990s. Any statement regarding the eventual long-term changes in surface water extent should be taken with caution, especially since the record is short and considering the corrections applied to the global emissivities in section 2.3. However, we note that the decreasing trend occurs until summer 2000, so it is not associated with the correction applied to the emissivities after 2001. In addition, a slight decrease in the surface water extent was also observed when looking at the original 8 year data set, 1993–2000 (Figure 1), and was shown to agree well with observed atmospheric methane anomalies [*Dlugokencky et al.*, 2001; *Bousquet et al.*, 2006]. We carefully checked the different individual satellite observations used as inputs to the methodology and no particular behavior was observed in the NDVI-AVHRR or the ERS measurements (over 8 years) related to these decrease observations at the global scale.

[46] Given the absence of other global, multiyear inundation estimates, the seasonal and interannual variabilities of our multisatellite inundation results are evaluated by comparison with related hydrological variables such as continental water height (rivers, lakes, floodplains, and other wetlands) as measured in situ or by satellite altimetry, in situ river discharge for large watersheds, and precipitation.

## 4. Evaluation Over Inland Surface Water Bodies and Large River Basins

[47] To evaluate the seasonal and interannual variations in the surface water extent, we compare our results with other related variables: water heights in rivers, floodplains, and wetlands, as measured by satellite altimetry, and precipitation and in situ river discharge for large watersheds such as the Amazon, the Congo, the Yellow River, and large Siberian rivers. For the period 2003–2004 the data set has already been compared with GRACE total water storage estimates and simulated surface water storage from WGHM and shows good agreement [*Papa et al.*, 2008b].

### 4.1. Comparison With Water Level Estimates From the Topex-Poseidon Altimeter

[48] The T/P radar altimeter is a joint French and U.S. mission with the first dual-frequency sensor whose primary goal is to perform accurate measurements of the ocean surface topography [*Fu and Cazenave*, 2001]. It operates in the Ku and C band, at frequencies (wavelengths) of 13.6 GHz (2.3 cm) and 5.3 GHz (5.8 cm), respectively. During its 10-day repeat cycle the T/P altimeter provides along-track nadir measurements of the Earth surface elevation (ocean and continental surfaces) between 66°N and 66°S latitude since it was launched in October 1992. Radar altimetry entails vertical range measurements between the satellite and the Earth surface, and water levels are given by the difference between the satellite orbit information and the range (or altimetric height) [*Fu and Cazenave*, 2001]. Radar altimeter water level series have been shown to be precise enough for continental water studies [*Birkett*, 1998; *Birkett*

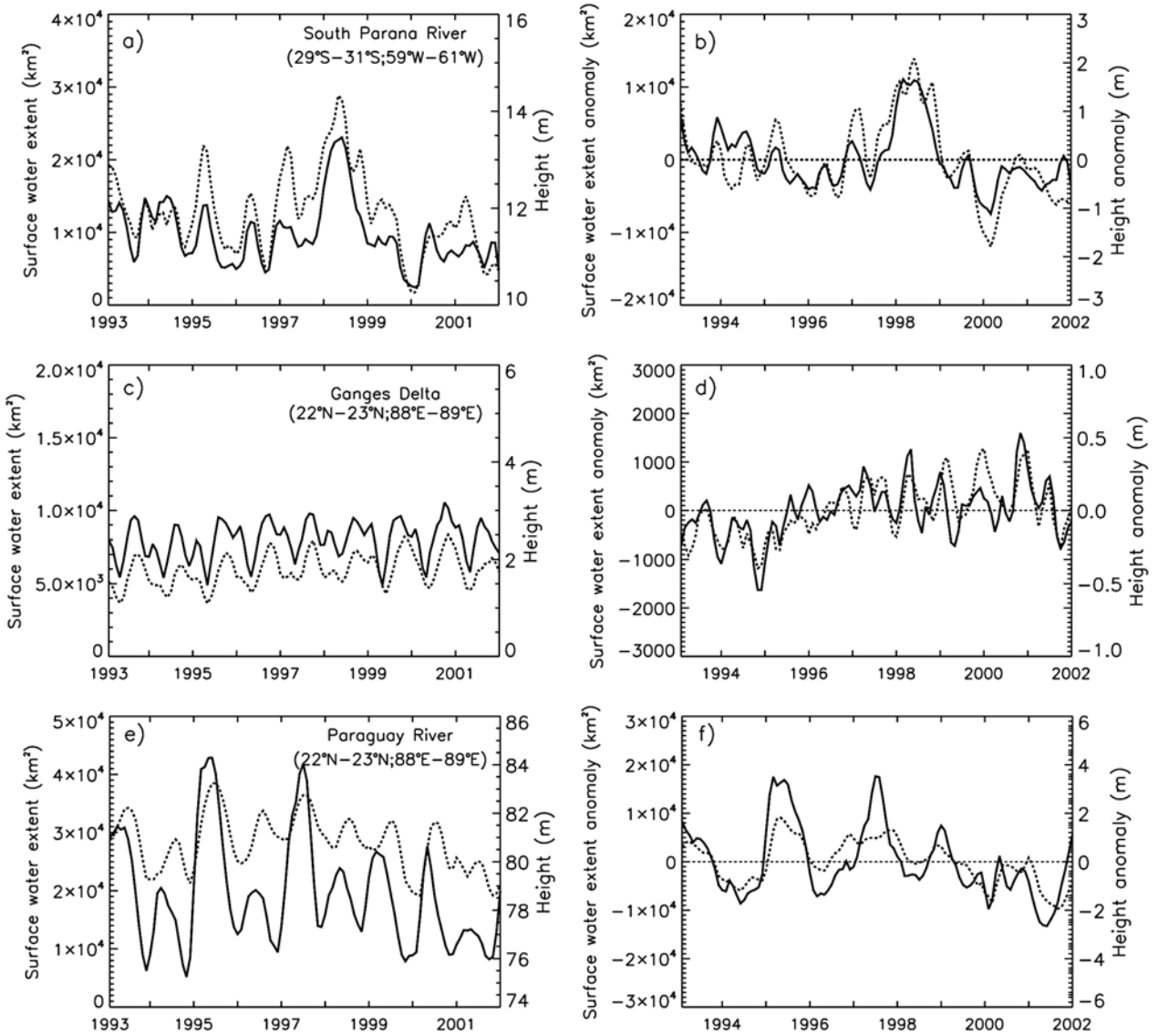


**Figure 9.** Correspondence between the monthly mean surface water extent and the altimeter-derived water height for the southern Parana River, the Ganges Delta, and the Paraguay River. (a) Monthly satellite-derived surface water extent (solid line, left axis) and water level derived from the Topex-Poseidon altimeter (dashed line, right axis) for 1993–2001. (b) Deseasonalized anomalies (obtained by subtracting the 12-year mean monthly value from individual months). A moving average of ±1 month is applied to all curves.

*et al.*, 2002; *Cretaux et al.*, 2006] and evaluated intensively against in situ gauge stations providing water level heights [*Calmant et al.*, 2008]. In this study we use the T/P-derived river/inundation and lake level heights from *Gennero et al.* [2005] (available at http://www.legos.obs-mip.fr/en/soa/hydrologie/hydroweb/), which provides consistent and accurate (precision of ~10 cm over open water to ~50 cm over large vegetated areas) river/inundation level heights from 1993 to 2001, before the orbit of T/P was changed. Note that the altimeter water level estimate and the multi-satellite extent product are completely independent, being estimated from different measurements and methodologies.

[49] Surface water extent and water height are two related characteristics of the surface water that, combined with topographic information, could provide an estimate of the water storage in the flooded plain [*Frappart et al.*, 2008]. *Prigent et al.* [2007] already showed that regardless of the environment, the seasonal and interannual variation patterns of the satellite-derived surface water extent and water level agree very well over 1993–2000. In the present study the variations of the surface water extent and their anomalies for the 10 years are compared systematically with the water level estimates.

[50] Figure 9 displays the 9 year time series for three locations representative of a variety of rivers and environments. The surface water extent estimates are averaged over the region around the altimeter measurement locations. For the three locations, there is a strong agreement between the

two data sets for the seasonal cycle and the interannual variability over the 10 years, even in environments of complex variability. Over the southern Parana, for instance (Figures 9a and 9b), very good agreement is observed, including during the exceptional 1997–1998 El Niño event, with a correlation of 0.82 (for this section, 108 months are used to calculate the linear correlation coefficient, giving $p < 0.01$, with $R > 0.23$) between the satellite-derived water extent and the altimetric river height during 1993–2001 and a correlation of 0.80 between their deseasonalized anomalies. Over the Ganges Delta, both data sets exhibit very similar variations ($R = 0.78$) and both extent and water height show a slight increase (Figures 9c and 9d), with a similar proportional rate of increase. For the Paraguay River (Figures 9e and 9f) the high peaks observed in the anomaly in 1995 and 1997 are well reproduced, although the magnitude observed in the water extent in 1997 is not as strong as that in the altimeter signal. The correlation between the satellite-derived water extent and the altimetric river height over 1993–2001 is 0.81 with a lag of 1 month (the extent preceding the height) and 0.80 with a 1 month lag between their deseasonalized anomalies.

[51] Many other locations (not shown) in different river basins also confirm the similar behavior in the surface water extent and river level height variations. After 2002 the Jason-1 mission replaced the T/P radar altimeter. Unfortunately, the Jason-1 radar altimeter does not provide measurements over continents and continental water bodies so the time series cannot be extended after 2002. We also investigate the use of the European Space Agency (Paris, France) ERS-2/Envisat altimeters, which provide longer time series of water level heights every 35 days during 1995–2009 and with a better accuracy, thanks to a special retracking technique. However, at the time of writing, no long time series from these altimeters has been made available to us. Only comparisons with Envisat radar altimeter data over 2003–2004, along with GRACE measurements [*Papa et al.*, 2008b], for the Amazon and the Ganges were made (not shown), and good agreement between the data sets was also observed.

### 4.2. Comparison With Rain Estimates, In Situ River Discharge, and Height Over Large River Basins

[52] The inundation characteristics depend on the distribution and intensity of precipitation as well as on the land surface properties and temperatures, which control how precipitation is partitioned among evaporation, storage at the surface and at depth, and runoff/discharge. Flooding can occur in response to locally intense precipitation as well as snow melt or heavy precipitation at upstream locations. In this case, inundation and precipitation are separated in both time and space. Temperatures play a role in the evaporation of the water stored in the river channels and floodplains. Keeping this in mind, we examine the relationship at the basin scale among the satellite-derived surface water extent, precipitation, and river discharge (when available) for several large river basins: the Amazon, the Congo, the Yellow River, and the large Siberian rivers. In situ discharge data overlapping in time with the surface water extent estimates are available for only a few river systems worldwide. In this study we can compare the surface water extent to the discharge of the Amazon River (1993–2004), the Congo (1993–2001), the Ob and the Yenissey rivers (1993–2004), and the Yellow River (1993–2004). For the precipitation we use the GPCC (Global Precipitation Climatology Centre) products. GPCC, established in 1989 by the World Climate Research Program, provides monthly data sets based on surface rain gauges that quantify the distribution of precipitation over the global land surface [*Rudolf and Schneider*, 2005]. GPCC is the in situ component of the World Climate Research Programme Global Precipitation Climatology Project [*Adler et al.*, 2003]. In this section we consider the basin-total monthly surface water extent and the basin-averaged monthly mean precipitation. To delineate the river basins, the template of the major river basins from total runoff integrating pathways [*Oki and Sud*, 1998] is adopted.

#### 4.2.1. The Amazon River Basin

[53] Figure 10 compares the surface water extent, precipitation, in situ river discharge and height, and altimeter-derived river height over the Amazon basin. The Amazon basin shows strong seasonal and interannual variations in precipitation, surface water extent, and discharge. The time series of the Amazon River discharge, which comprises 20% of the world's total continental runoff [*Richey et al.*, 1989], is closely linked to the total amount of satellite-derived surface water extent in the whole basin (Figure 10a), with a maximum lagged correlation of 0.90 (144 months is used to calculate the linear correlation coefficient, giving $p < 0.01$, with $R > 0.21$) with the extent preceding by 1 month the in situ discharge obtained from the Brazilian Water National Agency (Figure 10a). The lagged correlation between the deseasonalized anomalies of these two variables is 0.59 ($p < 0.01$). The temporal pattern indicates alternatively wet and dry events associated with the El Niño/La Niña phenomena as already described by *Prigent et al.* [2007]. Each year the precipitation often precedes the inundation; for the entire Amazon basin the lagged correlation between the surface water extent and the basin-averaged precipitation reaches 0.86, with rain preceding the water extent by 2 months. Part of the inundation change is likely due to precipitation events in upstream locations (but also to snow and glaciers melting) that do not flood but contribute to the water discharged from the entire basin [*Papa et al.*, 2006b, 2007; *Prigent et al.*, 2007].

[54] For a location such as Obidos (Figure 10b), 800 km upstream from the river mouth in the state of Para, variations in surface water extent are similarly consistent with river height measured in situ and by the T/P altimeter (available from 1993 to 2002 only; see section 4.1). After 2002 the time series anomalies reveal a slight decrease in the total surface water extent of the Amazon basin, which coincides also with a slight decrease in the Amazon in situ river discharge. Using recent gravimetric satellite measurements that provide the total continental water mass change (soil moisture, surface water, snow, and groundwater), water mass loss has been observed over several basins between 2003 and 2005, with a significant decrease over the Amazon, >20% of the total water mass loss over the 27 major basins that were studied [*Ramillien et al.*, 2008]. The declines in surface water extent derived from our data set and in river discharge are compatible with this observed water mass loss.

#### 4.2.2. Comparisons With Other Large River Basins

[55] Figure 11 compares the times series of the surface water extent and in situ river discharge in four large river

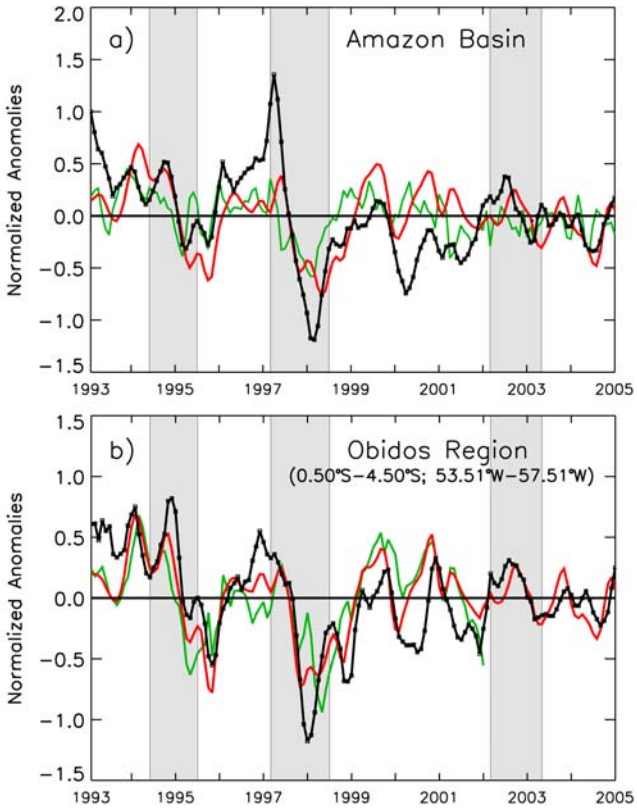


**Figure 10.** Correspondence among the satellite-derived monthly mean surface water extent, in situ river discharge and height, and rain gauge measurements in the Amazon. Normalized deseasonalized anomalies (obtained by subtracting the 12-year mean monthly value from individual months and dividing by the standard deviations of the raw time series). (a) For the entire Amazon basin: the black line is the satellite-derived surface water extent, the red line is the in situ river discharge from the Brazilian Water National Agency, and the green line is the basin mean precipitation from the Global Precipitation Climatology Centre. (b) For Obidos, Para, Brazil, located 800 km upstream from the mouth of the Amazon: the black line is the satellite-derived surface water extent averaged for a 4° × 4° region centered at Obidos, the red line is the in situ river height measured at Obidos, and the green line is the altimeter-derived river water height near Obidos (2.51°S, 56.50°W) from 1993 to 2002. A moving average of ±1 month is applied to all curves. The shading indicates El Niño events.

basins: two rivers in Siberia, the Ob and the Yenisey, the Congo basin in Africa, and the Yellow River in China. For the Ob and the Yenisey, monthly river discharges from 1993 to 2004 are available in the archives of the R-Arctic project (http://www.r-arcticnet.sr.unh.edu/v4.0/index.html). The monthly river discharge from the Congo (1993–2002) comes from the Global Runoff Data Center (Koblenz, Germany) database (http://www.bafg.de/GRDC/). The discharge data for the Yellow River are documented in the annual report by the Hydrological Bureau and are available at the Web site of the Ministry of Water Resources of China (http://www.hydroinfo.gov.cn/zyysq/index.htm) and in *Cong et al.* [2009]. For this river, only the annual mean river discharge is available to us for 1993–2004.

[56] For both Arctic rivers, Figures 11a and 11b show a good agreement between the surface water extent and the river discharge (both time series are normalized deseasonalized anomalies). Over 12 years the correlations between the two monthly variables are very high, at $R = 0.89$ ($p < 0.01$) for the Ob River basin and $R = 0.79$ ($p < 0.01$) for the Yenisey with a 1 month lag, the inundation preceding the river discharge. For the Ob River the positive and negative peaks (especially the two exceptional ones in 1995 and 2002) in the in situ discharge are well captured by the inundation estimates. The Congo (Figure 11c) is an interesting case in terms of seasonal flood dynamics because its basin is almost equally distributed between the Northern and the Southern hemispheres (~38% of the Congo basin is situated in the Northern Hemisphere, but only ~12% of the Amazon basin). The wet season starts in June for the northern part and in December for the southern part, represented by two annual peaks in the precipitation (not shown) and the surface water extent (except for the special event in 1998). The discharge and the surface water extent agree well in the seasonal and interannual cycles but have a maximum correlation of only 0.53, with the inundation preceding the discharge with a lag of 1 month. *Laraque et al.* [2001] reports that during the 1990s, the Congo River discharge dropped to the lowest level of the last century; however, for the period 1993–2004 no significant changes are observed in the total surface water extent or the river discharge. Note that the decrease in river discharge from 1999 to 2003 is not observed in the surface water extent data set. Finally, for the Yellow River basin (Figure 11d) the mean annual surface water extent and the mean annual river discharge agree very well for 1993–2004 ($R = 0.82$). The lower stage in the in situ river discharge from 1997 to 2002 is well reproduced in the surface water extent estimates as well as the positive anomaly in 2003.

## 5. Conclusion and Perspectives

[57] This study presents the first global data set that quantifies the monthly distribution of surface water extent and its variations at ~25 km sampling intervals over more than a decade, 1993–2004. The multisatellite methodology captures, at the global scale, the extent of episodic and seasonal inundations, wetlands, rivers, lakes, and irrigated agriculture, using passive (SSM/I) and active (ERS scatterometer) microwaves and visible and near-IR (AVHRR) observations. A satisfactory solution has been found to overcome the lack of scatterometer data after January 2001. An adequate correction was also applied to the extended SSM/I 1993–2004 emissivity data set after a problem in the time series starting in October 2001 was detected in the ancillary data used in the emissivity calculation.

[58] Twelve years (1993–2004) of the new estimates of global monthly water surfaces extent is now available. The surface water extent at the global scale shows a strong seasonal and interannual variability and an overall slight decrease over the 12 year record. This gradual decrease is particularly noticeable over the tropics from 1993 to 2000.

[59] At the global scale the satellite-derived surface water extent is compared with the GLWD of *Lehner and Doll*

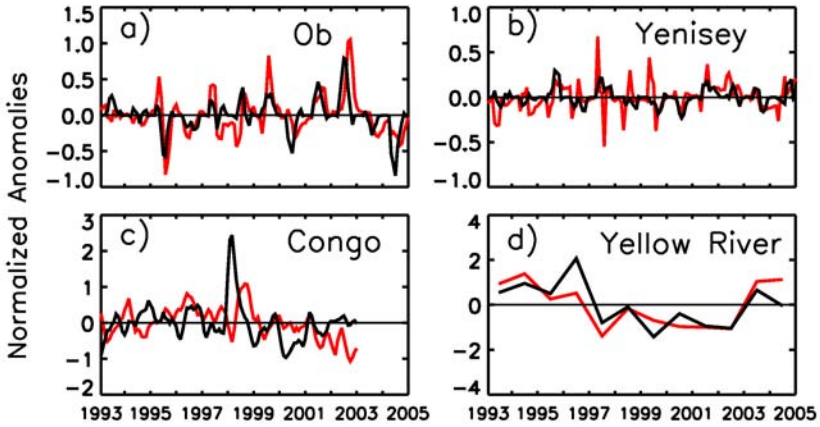


**Figure 11.** (a–c) Correspondence between the satellite-derived monthly mean surface water extent and the in situ river discharge for the Ob, the Yenisey, and the Congo rivers (normalized deseasonalized anomalies). (d) Correspondence between the annual mean surface water extent and the in situ river discharge for the Yellow River in China. A moving average of ±1 month is applied to all curves except in Figure 11d.

[2004]. Over inland water bodies and large river basins, the seasonal and interannual variations of the satellite-derived surface water extent and changes have been evaluated with other related hydrological variables: river and floodplain water height levels from altimeter measurements, rain rate estimates (GPCC), and in situ river discharge and height. For most cases the seasonal and interannual variations and changes observed in the surface water extent are consistent with variations in the other related hydrological variables. Over the Amazon basin, all variables agree exceptionally well.

[60] This unique global data set of surface water extent variations over more than a decade (available in the near future until 2008, when global land surface emissivities become available) removes a crucial obstacle to progress on several fundamental scientific questions and can now be used to improve our understanding of the hydrological process. In particular, combination with other data sets to derive crucial parameters, such as surface water storage, shows significant potentials [*Papa et al.*, 2008b]. *Frappart et al.* [2008] computed maps of monthly surface water volume change over 8 successive years (1993–2000) by combining the surface water extent data set with altimetric observations and in situ data over the basin of the Rio Negro. This study can now be extended to more years and more river basins. Development of the same technique is under investigation for other large watersheds such as the Mississippi, the Mackenzie, the Ob, the Niger, the Ganges, and the Amazon. In parallel, a new technique that combines the surface water extent with digital elevation models (e. g., GTOPO-30) to retrieve surface water volume change at the global scale is also under investigation. Surface water volume change, together with GRACE-derived total water storage, precipitation, and river discharge and upcoming soil moisture products derived from the Soil Moisture and Ocean Salinity (SMOS) and Soil Moisture Active & Passive (SMAP) missions, will provide the opportunity to separate the total water storage into its different components. It will offer new opportunities to analyze the variations in the water balance equation at the basin-continental scale and improve model representation of global surface water dynamics. Moreover, a global surface water volume change data set is central to understanding the role of continental water in the sea-level rise. Although progress has been made in quantifying the two primary contributors to sea-level rise, namely, thermal expansion due to ocean warming and melting glaciers and ice sheets, large uncertainties remain regarding the effect of changes in continental water storage, despite recent results from gravimetric satellite missions. Our new estimates of surface water extent provide the opportunity to produce future data sets of variations in global surface water volumes, quantify fluctuations in river discharge to the ocean, and better understand the role of terrestrial water in the present sea-level rise.

[61] **Acknowledgments.** We thank Bertrand Decharme at Météo-France for providing us the in situ discharge of the Congo River and Eric Leuliette (LSA-NOAA) for helping us with the Amazon River discharge measurements from the Brazilian Water National Agency (Agência Nacional de Águas). We thank Andreas Güntner at GFZ-Postdam, who suggested the use of the GPCC precipitation products. We also thank Bernhard Lehner, McGill University, for providing us with the GLWD data set. This research was supported by NASA NEWS grant NNDX7AO90E, managed by Dr. Jared K. Entin, by a European Union (FP6) Integrated Project called WATCH (contract no. 036946; project coordinated by Dr. Richard Harding), and by the program IMPACT-BOREAL of the French Agence Nationale pour la Recherche.

[62] We thank two anonymous reviewers for their constructive comments and suggestions.

## References

Adler, R. F., G. J. Huffman, A. Chang, R. Ferraro, P. Xie, J. Janowiak, B. Rudolf, U. Schneider, S. Curtis, D. Bolvin, A. Gruber, J. Susskind, and P. Arkin (2003), The Version 2 Global Precipitation Climatology Project (GPCP) monthly precipitation analysis 1979-present, *J. Hydrometeorol.*, *4*, 1147–1167.

Alsdorf, D. E., and D. P. Lettenmaier (2003), Tracking fresh water from space, *Science*, *301*, 1492–1494.

Alsdorf, D. E., E. Rodríguez, and D. P. Lettenmaier (2007a), Measuring surface water from space, *Rev. Geophys.*, *45*, RG2002, doi:10.1029/2006RG000197.

Alsdorf, D., P. Bates, J. Melack, M. Wilson, and T. Dunne (2007b), Spatial and temporal complexity of the Amazon flood measured from space, *Geophys. Res. Lett.*, *34*, L08402, doi:10.1029/2007GL029447.

Armstrong, R. L., and M. J. Brodzik (2005), Northern Hemisphere EASE-Grid weekly snow cover and sea ice extent version 3, National Snow and Ice Data Center, Boulder, Colo.

Berge-Nguyen, M., J. F. Crétaux, and S. Calmant (2008), Combining of radar altimetry and MODIS for the monitoring of flood events: application to the Inner Niger delta, presented at Observing and Forecasting the Ocean, OSTST meeting, Nice, France, Nov. 2008.

Birkett, C. M. (1998), Contribution of the TOPEX NASA radar altimeter to the global monitoring of large rivers and wetlands, *Water Resour. Res.*, *34*(5), 1223–1239.

Birkett, C. M., L. A. K. Mertes, T. Dunne, M. H. Costa, and M. J. Jasinski (2002), Surface water dynamics in the Amazon basin: Application of satellite radar altimetry, *J. Geophys. Res.*, *107*(D20), 8059, doi:10.1029/2001JD000609.

Bousquet, P., et al. (2006), Contribution of anthropogenic and natural sources to atmospheric methane variability, *Nature*, *443*, 439–443, doi:10.1038/nature05132.

Calmant, S., F. Seyler, and J. F. Cretaux (2008), Monitoring continental surface waters by satellite altimetry, *Surv. Geophys.*, *29*(4–5), 247–269, doi:10.1007/s10712-008-9051-1.

Cao, Z., et al. (2002), On the physical process associated with water budget and discharge over the Mackenzie basin during 1994/95 water year, *Atmopshere-Ocean*, *40*(2), 125–143.

Cazenave, A., P. C. D. Milly, H. Douville, J. Benveniste P. Kosuth, and D. P. Lettenmaier (2004), Space techniques used to measure change in terrestrial waters, *Eos Trans. AGU*, *85*(6), 59.

Coe, M. T. (2000), Modeling terrestrial hydrological systems at the continental scale: Testing the accuracy of an atmospheric GCM, *J. Clim.*, *13*, 686–704.

Coe, M. T., M. H. Costa, A. Botta, and C. Birkett (2002), Long-term simulations of discharge and floods in the Amazon Basin. *J. Geophys. Res. 107*(D20), 8044, doi:10.1029/2001JD000740.

Cogley, J. (2003), GGHYDRO-Global Hydrographic Data, release 2.3, Tech. Note 2003-1, Dept. of Geogr., Trent Univ., Peterborough, Ont., Canada.

Cong, Z., D. Yang, B. Gao, H. Yang, and H. Hu (2009), Hydrological trend analysis in the Yellow River basin using a distributed hydrological model, *Water Resour. Res.*, *45*, W00A13, doi:10.1029/2008WR006852.

Cracknell, A. P. (1997), *The Advanced Very High Resolution Radiometer*, 534 pp., Taylor and Francis, London.

Crétaux, J. F., and C. Birkett (2006), Lake studies from satellite altimetry, *C. R. Geosci.*, *338*, 1098–1112, doi:10.1016/J.crte.2006.08.002.

Decharme, B., H. Douville, C. Prigent, F. Papa, and F. Aires (2008), A new river flooding scheme for global climate applications: Off-line validation over South America, *J. Geophys. Res.*, *113*, D11110, doi:10.1029/2007JD009376.

Dlugokencky, E., B. Walter, K. Masarie, P. Lang, and E. Kasischke (2001), Measurements of an anomalous global methane increase during 1998, *Geophys. Res. Lett.*, *28*(3), 499–502.

Finlayson, C. M., N. C. Davidson, A. G. Spiers, and N. J. Stevenson (1999), Global wetland inventory & current status and future priorities, *Mar. Freshwater Res.*, *50*, 717–727.

Frappart, F., F. Papa, J. S. Famiglietti, C. Prigent, W. B. Rossow, and F. Seyler (2008), Interannual variations of river water storage from a multiple satellite approach: A case study for the Rio Negro River basin, *J. Geophys. Res.*, *113*, D21104, doi:10.1029/2007JD009438.

Fu, L. L., and A. Cazenave (2001), *Satellite aAltimetry and Earth Sciences, A Handbook of Techniques and Applications*, International Geophysics Series, 69, Academic Press, San Diego, Calif.

Gedney, N., P. M. Cox, and C. Huntingford (2004), Climate feedback from wetland methane emission, *Geophys. Res. Lett.*, *31*, L20503, doi:10.1029/2004GL020919.

Gennero, M. C., J. F. Cretaux, M. Berge NGuyen, C. Maheu, K. Do Minh, S. Calmant, and A. Cazenave (2005), Surface water monitoring by satellite altimetry, Laboratoire d'Etudes en Géodésie et Oceanographie Spatiale, Toulouse, France. (Available at: http:/ /legos.obs-mip.fr/soa/hydrologie/hydroweb/)

Giddings, L., and B. J. Choudhury (1989), Observation of hydrological feature with Nimbus-7 37 GHz data applied to South America, *Int. J. Remote Sens.*, *10*, 1673–1686.

Gleick, P. H. (2003), Global freshwater resources: Soft-path solutions for the 21st century, *Science*, *302*, 1524–1528.

Hess, L. L., J. M. Melack, E. M. L. M. Novob, C. C. F. Barbosac, and M. Gastil (2003), Dual-season mapping of wetland inundation and vegetation for the central Amazon basin, *Remote Sens. Environ.*, *87*, 404–428.

Houweling, S., T. Kamisnki, F. Dentefer, J. Lelieveld, and M. Heinmann (1999), Inverse modeling of methane sources and sinks using the adjoint of a global transport model, *J. Geophys. Res.*, *104*, 26,137–26,160.

IPCC (2007), Climate Change 2007: The physical science basis, *Contribution of Working Group I to the Fourth Assessment Report of the Intergovernmental Panel on Climate Change*, edited by S. Solomon et al., Cambridge University Press, Cambridge, U. K.

James, M. E., and S. N. V. Kalluri (1994), The Pathfinder AVHRR land data set: An improved coarse resolution data set for terrestrial monitoring, *Int. J. Remote Sens.*, *15*, 3347–3364.

Kalnay, E., et al. (1996), The NCEP/NCAR 40-year reanalysis project, *Bull. Am. Meteorol. Soc.*, *77*, 437–470.

Kidwell, K. B. (2000), *NOAA KLM User's Guide*, National Oceanic and Atmospheric Administration, Boulder, Colo.

Krinner, G. (2003), Impact of lakes and wetlands on boreal climate, *J. Geophys. Res.*, *108*(D16), 4520, doi:10.1029/2002JD002597.

Laraque, A., G. Mahe, D. Orange, and B. Marieu (2001), Spatiotemporal variations in hydrological regimes within Central Africa during the XXth century, *J. Hydrol.*, *25*, doi:10.1016/S0022-1694(01)00340-7.

Lehner, B., and P. Doell (2004), Development and validation of a global database of lakes, reservoirs and wetlands, *J. Hydrol.*, *296*, 1–22.

Loveland, T. R., B. C. Reed, J. F. Brown, D. O. Ohlen, J. Zhu, L. Yang, and J. W. Merchant (2000), Development of a global land cover characteristics dat abase and IGBP DISCover from 1-km AVHRR data, *Int. J. Remote Sens.*, *21*, 1303–1330.

Marburger, J. H., and J. B. Bolten (2005), FY 2007 administration research and development budget priorities, Memo. M-05-18, Executive Office of U.S. President, Washington, D. C. (Available at: http://www.ostp.gov/html/budget/2007/ostp_omb_guidancememo_FY07.pdf)

Matthews, E. (2000), *Wetlands in Atmospheric Methane: Its Role in the Global Environment*, pp. 202–233, edited by M. A. K. Khalil, Springer-Verlag, New York.

Matthews, E., and I. Fung (1987), Methane emission from natural wetlands: Global distribution, area, and environmental characteristics of sources, *Global Biogeochem. Cycles*, *1*, 61–86.

Matthews, E., I. Fung, and J. Lerner (1991), Methane emission from rice cultivation: Geographic and seasonal distribution of cultivated areas and emissions, *Global Biogeochem. Cycles*, *5*, 3–24.

Mialon, A., A. Royer, and M. Fily (2005), Wetland seasonal dynamics and interannual variability over northern high latitudes derived from microwave satellite data, *J. Geophys. Res.*, *110*, D17102, doi:10.1029/2004JD005697.

Oki, T., and C. Sud (1998), Design of Total Runoff Integrating Pathways (TRIP)-A global river channel network, *Earth Interactions*, *2*, 1–37.

Papa, F., B. Legresy, N. M. Mognard, E. G. Josberger, and F. Remy (2002), Estimating terrestrial snow depth with the Topex-Poseidon altimeter and radiometer, *IEEE Trans. Geosci. Remote Sens.*, *40*, 2162–2169, doi:10.1109/TGRS.2002.802463.

Papa, F., B. Legresy, and F. Remy (2003), Use of the Topex-Poseidon dual-frequency radar altimeter over land surfaces, *Remote Sens. Environ.*, *87*, 136–147, doi:10.1016/S0034-4257(03)00136-6.

Papa, F, C. Prigent, W. B. Rossow, B. Legresy, and F. Remy (2006a), Inundated wetland dynamics over boreal regions from remote sensing: The use of Topex-Poseidon dual-frequency radar altimeter observations, *Int. J. Remote Sensing*, *27*, 4847–4866, doi:10.1080/01431160600675887.

Papa, F., C. Prigent, F. Durand, and W. B. Rossow (2006b), Wetland dynamics using a suite of satellite observations: A case study of application and evaluation for the Indian Subcontinent. *Geophys. Res. Lett.*, *33*, L08401, doi:10.1029/2006GL025767.

Papa, F., C. Prigent, and W. B. Rossow (2007), Ob' River flood inundations from satellite observations: A relationship with winter snow parameters and river runoff, *J. Geophys. Res.*, *112*, D18103, doi:10.1029/2007JD008451.

Papa, F., C. Prigent, and W. B. Rossow (2008a), Monitoring flood and discharge variations in the large Siberian rivers from a multi-satellite technique, *Surv. Geophys.*, *29*(4–5), 297–317, doi:10.1007/s10712-008-9036-0.

Papa, F., A. Güntner, F. Frappart, C. Prigent, and W. B. Rossow (2008b), Variations of surface water extent and water storage in large river basins: A comparison of different global data sources, *Geophys. Res. Lett.*, *35*, L11401, doi:10.1029/2008GL033857.

Prigent, C., W. B. Rossow, and E. Matthews (1997), Microwave land surface emissivities estimated from SSM/I observations, *J. Geophys. Res.*, *102*, 21867–21890.

Prigent, C., E. Matthews, F. Aires, and W. B. Rossow (2001a), Remote sensing of global wetland dynamics with multiple satellite data sets, *Geophys. Res. Lett.*, *28*, 4631–4634.

Prigent, C., F. Aires, W. B. Rossow, and E. Matthews (2001b), Joint characterization of vegetation by satellite observations from visible to microwave wavelength: A sensitivity analysis, *J. Geophys. Res.*, *106*, 20,665–20,685.

Prigent, C., F. Aires, and W. B. Rossow (2006), Land surface microwave emissivities over the globe for a decade, *Bul. Am. Meteorol. Soc.*, *87*, 1573–1584, doi:10.1175/BAMS-87-11-1573.

Prigent, C., F. Papa, F. Aires, W. B. Rossow, and E. Matthews (2007), Global inundation dynamics inferred from multiple satellite observations, 1993–2000, *J. Geophys. Res.*, *112*, D12107, doi:10.1029/2006JD007847.

Ramillien, G., F. Frappart, A. Cazenave, and A. Güntner (2005), Time variations of the land water storage from an inversion of 2 years of GRACE geoids, *Earth Planet. Sci. Let.*, *235*, 283–301.

Ramillien, G., et al. (2008), Land water storage contribution to sea level from GRACE geoid data over 2003–2006, *Global Planet Change*, *60*, 381–392.

Rango, A. (1996), Spaceborne remote sensing for snow hydrology applications, *Hydrol. Sci. J.*, *41*(4), 477–494.

Richey, J. E., C. Nobre, and C. Deser (1989), Amazon River discharge and climate variability: 1903 to 1985, *Science*, *6*(4926), 101–103, doi:10.1126/science.246.4926.101.

Richey, J. E., J. M. Melack, A. K. Aufdenkampe, V. M. Ballester, and L. Hess (2002), Outgassing from Amazonian rivers and wetlands as a large tropical source of atmospheric $CO_2$, *Nature*, *416*, 617–620.

Ringeval, B., N. de Noblet-Ducoudré, P. Ciais, P. Bousquet, C. Prigent, F. Papa, and W. B. Rossow (2010), An attempt to quantify the impact of changes in wetland extent on methane emissions on the seasonal and interannual time scales, *Global Biogeochem. Cycles*, *24*, GB2003, doi:10.1029/2008GB003354.

Rodell, M., J. Chen, H. Kato, J. Famiglietti, J. Nigro, and C. Wilson (2006), Estimating ground water storage changes in the Mississippi river basin using GRACE, *Hydrogeol. J.*, *15*, 159–166, doi:10.1007/s10040-006-0103-7.

Rossow, W. B., and R. A. Schiffer (1999), Advances in understanding clouds from ISCCP, *Bull. Am. Meteorol. Soc*., *80*, 2261–2287.

Rudolf, B., and U. Schneider (2005), Calculation of gridded precipitation data for the global land-surface using *in-situ* gauge observations, in *Proceedings,* 2nd *Workshop of the Int. Precipitation Working Group IPWG, Monterey October 2004*, pp. 231–247, EUMETSAT, Darmstadt, Germany.

Sakamoto, T., N. Van Nguyenb, A. Koteraa, H. Ohnoa, N. Ishitsukaa, and M. Yokozawaa (2007), Detecting temporal changes in the extent of annual flooding within the Cambodia and the Vietnamese Mekong Delta from MODIS time series imagery, *Remote Sens. Environ.*, *109*(3), 295–313, doi:10.1016/j.rse.2007.01.011.

Siebert, S., J. Hoogeveen, and K. Frenken (2006), Irrigation in Africa, Europe and Latin America-Update of the Digital Global Map of Irrigation Areas to Version 4, Frankfurt Hydrology Paper 05, Institute of Physical Geography, University of Frankfurt, Frankfurt am Main, Germany, and Food and Agriculture Organization of the United Nations, Rome.

Sippel, S. J., S. K. Hamilton, J. M. Melack, and E. M. M. Novo (1998), Passive microwave observations of inundation area and the area/stage relation in the Amazon River floodplain, *Int. J. Remote Sens.*, *19*, 3055–3074.

Smith, L. C. (1997), Satellite remote sensing of river inundation area, stage and processes: A review, *Hydrol. Processes*, *11*, 1427–1439.

Smith, L. C., and D. E. Alsdorf (1998), Control on sediment and organic carbon delivery to the Arctic Ocean revealed with space-borne synthetic aperture radar: Ob' River, Siberia, *Geology*, *26*, 395–398.

Tapley, B. D., S. Bettadpur, J. C. Ries, P. F. Thompson, and M. Watkins (2004a), GRACE measurements of mass variability in the Earth system, *Science*, *305*, 503–505.

Tapley, B. D., S. Bettadpur, M. Watkins, and C. Reigber (2004b), The Gravity Recovery and Climate Experiment: Mission overview and early results, *Geophys. Res. Lett.*, *31*, L09607, doi:10.1029/2004GL019920.

Tucker, C. J., J. E. Pinzon, M. E. Brown, D. Slay cxback, E. W. Pak, R. Mahoney, E. Vermote, and N. El Saleous (2005), An extended AVHRR 8-km NDVI data set compatible with MODIS and SPOT vegetation NDVI data, *Int J. Remote Sens.*, *26*(20), 4485–5598.

United Nations (2004), International Decade for Action, "Water for Life, " 2005–2015, General Assembly Resolution A/RES/58/217, United Nations, New York. (Available at www.un.org/Depts/dhl/resguide/r58.htm)

Vörösmarty, C. J., P. Green, J. Salisbury, and R. B. Lammers (2000), Global water resources: Vulnerability from climate changes and population growth, *Science*, *289*, 284–288.

Vörösmarty, C. J., L. D. Hinzman, B. J. Peterson, D. H. Bromwich, L. C. Hamilton, J. Morison, V. E. Romanovsky, M. Sturm, and R. S. Webb (2001), The hydrologic cycle and its role in arctic and global environmental change: a rationale and strategy for synthesis study, 84 pp., Arctic Res. Consortium of the United States, Fairbanks, Alaska.

Zhang, Y., W. B. Rossow, and P. W. Stackhouse Jr. (2006), Comparison of different global information sources used in surface radiative flux calculation: Radiative properties of the near-surface atmosphere, *J. Geophys. Res.*, *111*, D13106, doi:10.1029/2005JD006873.

F. Aires, CNRS, Laboratoire de Météorologie Dynamique, Université Pierre et Marie Curie, Paris, France.

C. Jimenez and C. Prigent, Laboratoire d'Etudes du Ryonnement et de la Matière en Astrophysique, CNRS, Observatoire de Paris, Paris, France.

E. Matthews, NASA Goddard Institute for Space Studies, 2880 Broadway, New York, NY 10025, USA.

F. Papa (corresponding author) and W. B. Rossow, NOAA Cooperative Remote Sensing Science and Technology Center, City College of New York, 160 Convent Av., New York, NY 10031, USA. (papa@ee.ccny.cuny.edu; fpapa@giss.nasa.gov)